PHYSICAL REVIEW D VOLUME 24, NUMBER 5 1 SEPTEMBER 1981

Rapid Communications

The Rapid Communications section is intended for the accelerated publication of important new results. Manuscripts submitted to this section are given priority in handling in the editorial office and in production. A Rapid Communication may be no longer than 3½ printed pages and must be accompanied by an abstract. Page proofs are sent to authors, but, because of the rapid publication schedule, publication is not delayed for receipt of corrections unless requested by the author.

Measurement of elastic ν_μ and $\bar{\nu}_\mu$ scattering on protons

P. Coteus, M. Diesburg, R. Fine, W. Lee, and P. Sokolsky
Columbia University, New York, New York 10027

R. Brown, S. Fuess, P. Nienaber, and T. O'Halloran, Jr.
University of Illinois, Urbana, Illinois 61801

Y. Y. Lee
Brookhaven National Laboratory, Upton, New York 11973
(Received 22 May 1981)

We have measured elastic ν_μ and $\bar{\nu}_\mu$ scattering on protons at the Brookhaven National Laboratory Alternating Gradient Synchrotron. We find $R_{\rm NC}=\sigma(\bar{\nu}_\mu p\to\bar{\nu}_\mu p)/\sigma(\nu_\mu p\to\nu_\mu p)=0.44\pm0.12$ and $R_{\nu_\mu}=\sigma(\nu_\mu p\to\nu_\mu p)/\sigma(\nu_\mu n\to\mu^- p)=0.11\pm0.03$. The elastic Q^2 distribution is in good agreement with present knowledge of form factors and the Weinberg-Salam model. We find $\sin^2\theta_W=0.26\pm0.06$.

We report on a measurement of

$$R_{\rm NC}=\sigma(\bar{\nu}_\mu p\to\bar{\nu}_\mu p)/\sigma(\nu_\mu p\to\nu_\mu p)\ ,$$

$$R_{\nu_\mu}=\sigma(\nu_\mu p\to\nu_\mu p)/\sigma(\nu_\mu n\to\mu^- p)\ ,$$

and the ν and $\bar{\nu}$ elastic Q^2 distributions. Previous measurements of these quantities have been reported by several groups.[1] The sample of data on which our measurements are based represents a significant improvement in statistics for $\bar{\nu}$.

The experiment was performed at the Brookhaven Alternating Gradient Synchrotron (AGS) neutrino beam. This is a horn-focused wide-band neutrino beam. Protons are fast extracted at a 28-GeV/c momentum and the rf structure preserved. This yields 12 30-ns-wide buckets/spill with a 220-ns separation between buckets. The detector consists of 154 6-ft × 6-ft × $\frac{1}{4}$-in.-thick aluminum plates separated into 22 spark-chamber modules. These are interspersed with 20 planes of plastic scintillator at $\frac{1}{2}$-radiation-length intervals. The detector is divided into a front and back half by a 72D18 air-gap magnet with a 6-ft vertical aperture. The detector is surrounded by overlapping scintillation counters covering $\sim 260°$ in azimuth. Their purpose is to detect any wide-angle tracks missed by the spark chambers. The detector is followed by a muon spectrometer consisting of six 8-ft-diameter magnetized iron toroids and eight 8-ft × 8-ft aluminum spark chambers. The chambers are photographed in narrow-angle stereo. Time-of-flight and pulse-height information are recorded for all scintillation counters.

The detector is located ~ 150 ft behind the primary iron shield and ~ 50 ft behind a secondary muon shield. The top and sides of the detector are shielded from neutrons by concrete but there is no significant shielding material directly in front of the chambers. The absence of mass in front of the detector implies that neutrons arriving at the detector have a flight path of > 50 ft, thus allowing separation of neutrinos from neutrons by time of flight for neutron momenta < 1.0 GeV.

The data sample on which this measurement is based represents 2×10^{18} p's for ν and 6×10^{18} p's for $\bar{\nu}$.

Data processing. All sparks on the film were digitized on the University of Illinois DOLLY system. A pattern-recognition program then found frames which had a spark pattern consistent with a minimum track length of four sparks. A manual scan of all frames found by the pattern-recognition program selected events in the topologies of interest (one- and two-straight-track events) and a straight-line fit was performed to the digitized sparks. The fitted track was

then associated with counter time-of-flight and pulse-height information. A final physicist scan was performed to reject events with associated shower or nuclear-breakup tracks at the vertex. The scanning efficiency was found to be $(96 \pm 1)\%$ averaged over all tracks.

Neutron background. Neutron background is expected from two sources: ν's interacting in the muon shield and producing neutrons, and neutrons from the primary proton interaction scattering in the air and earth and entering our apparatus. In both cases, neutrons will arrive out of time up to a momentum of 1.0 GeV/c.

Because $np \to np\pi^0$ events have a threshold at $P_n \sim 1.0$ GeV/c and will attenuate in our detector, the number of neutrons in the beam with $P_n > 1.0$ GeV/c can be determined by the flatness of the vertex distribution of $\nu p \to \nu p \pi^0$ candidates along the beam direction, and is found to be negligible.

We study the characteristics of the background by examining events in the first seven chambers where it is expected to be highest. The time-of-flight (TOF) spectrum for neutrons is flat. Most of the neutron background points downward, has a small angle with respect to the neutrino beam, and has lower momentum than the in-time signal. We make the following cuts: a fiducial cut of 4 ft × 4 ft and chambers 7–20, $P_p > 600$ MeV/c, and if $\theta_p < 30°$, then the proton must point upwards (600 cuts). This data sample consisting of ν_μ and $\bar{\nu}_\mu$ elastic candidates is used to form the ratio $R_{\rm NC}$ below. For purposes of measuring R_{ν_μ}, we use the back half of the detector to maximize the muon acceptance. A momentum cut of $P_p > 520$ MeV/c is the only cut here (520 cuts) since neutron background is much smaller for this sample. Figure 1 shows the folded TOF distribution for these samples. After a straight-line background subtraction, the number of neutrino-induced ν and $\bar{\nu}$ events is given in Table I.

Neutrino-induced background. There are two kinds of neutrino-induced backgrounds: charged-current (CC) events where the muon escapes detection, and neutral-current (NC) single-π events. The contamination due to CC events can be studied directly using the wide-angle-muon (WAM) counters surrounding the detector. The efficiency and relative timing of these counters is studied by using CC events with leaving muons that hit a WAM counter. A search was performed for associated hits in the WAM counters for all elastic candidates. These events were assumed to be quasielastic events and were added to the two-prong sample to be discussed later.

Single-pion events can mimic elastic events in four ways: $\nu p(\pi^0)_{\rm invisible}$, $\nu p(\pi^-)_{\rm invisible}$, $\nu(p)_{\rm invisible}\pi^-$, and $\nu(n)_{\rm invisible}\pi^+$. In the latter two cases, the stopping track is a pion. We can estimate the background for these two cases by studying the pulse-height distribution of the tracks. Figure 2(b) shows the pulse-height distribution of protons from quasielastic events; Fig. 2(c) shows the minimum-ionizing pulse-height distribution. We have verified that π's have a minimum-ionizing distribution in our detector by studying a sample of $\mu^+ n \pi^-$ candidates where the π stops in the detector. Figure 2(a) shows the pulse-height distribution of the elastic candidates. A maximum-likelihood fit of the proton and minimum-ionizing distribution to the elastic distribution yields the pion contamination given in Table I. These numbers are consistent with expected numbers of single-pion events using the known single-pion cross sections and pion acceptances normalized to the observed number of quasielastic events in our data.

The probability that a charged pion is not detected either by the WAM's or the chambers is very small and is ignored in our analysis.

We study the background from $\nu p(\pi^0)_{\rm invisible}$ by

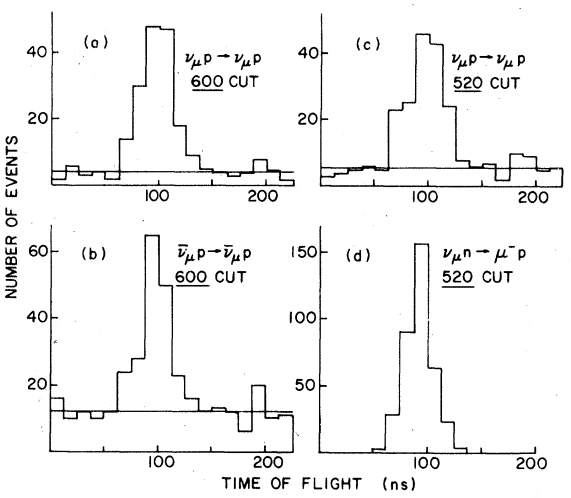

FIG. 1. Time of flight modulo 220 ns (rf spacing of extracted proton beam) for (a) $\nu_\mu p \to \nu_\mu p$ candidates; (b) $\bar{\nu}_\mu p \to \bar{\nu}_\mu p$ candidates, 600 cuts; (c) $\nu_\mu p \to \nu_\mu p$ candidates, 520 cuts; (d) $\nu_\mu n \to \mu^- p$ candidates, 520 cuts. Solid line indicates neutron subtraction.

TABLE I. Summary of elastic-candidate rates as a function of corrections.

	$\bar{\nu}$ (600 cuts)	ν (600 cuts)	ν (520 cuts)
In-time events	192	159	164
Neutrino induced	125	136	134
After WAM correction	125	117	116
Elastic candidates after pion subtraction	104	102	94

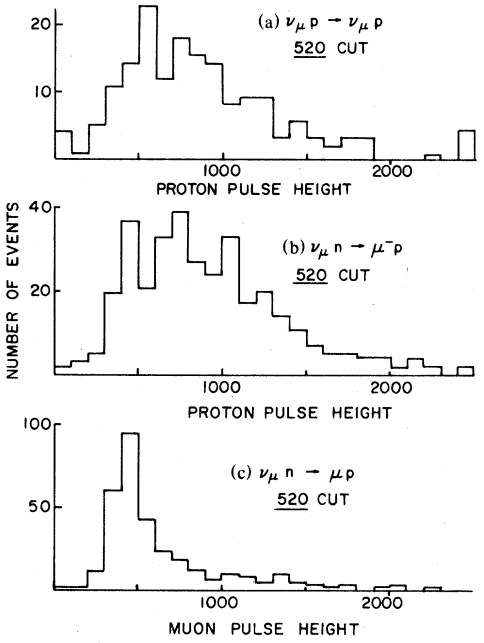

FIG. 2. Pulse-height distribution of in-time events for (a) $\nu_\mu p \rightarrow \nu_\mu p$ candidates, 520 cuts; (b) proton track of $\nu_\mu n \rightarrow \mu^- p$ candidates, 520 cuts; (c) muon track of $\nu_\mu n \rightarrow \mu^- p$ candidates.

scanning for events consistent with the $\nu p \pi^0$ ($\pi^0 \rightarrow \gamma\gamma$) topology. We study how often we miss a γ ray by examining events with at least one γ ray and seeing how often we miss the second γ ray. We estimate a total π^0 efficiency of 90%.

A final correction is due to $\bar{\nu}_\mu$ background in ν_μ data and ν_μ background in $\bar{\nu}_\mu$ data. This is studied by measuring the μ^+/μ^- ratio in the ν_μ and $\bar{\nu}_\mu$ CC data using the toroidal spectrometer. The flux contamination is found to be $(2.3 \pm 1.0)\%$ and $(4.6 \pm 0.8)\%$, respectively.

Quasielastic data. The selection of the quasielastic sample is similar to the elastic one. The sample consists of all two-prong events where one of the tracks satisfies the elastic proton cuts described above ($P_p > 520$). Only events with vertices in the back half of the detector are used. Elastic events with associated WAM hits are added to the sample. There is no neutron background. Single-pion background is estimated by studying the pulse-height and coplanarity distribution. The corrected number of quasielastic events is 384.

Flux ratio. In order to form the ratio of $\bar{\nu}/\nu$ cross sections, the $(\bar{\nu})$-flux energy dependence and ratio of fluxes must be known. The energy distribution of neutrino and antineutrino quasielastic events can be determined for small Q^2 [$Q^2 < 0.2$ (GeV/c)^2]. The toroidal muon spectrometer has an acceptance of 60% for these events. The neutrino energy is reconstructed from the muon momentum and angle. The observed event distributions imply that the ν and $\bar{\nu}$ fluxes have similar energy distributions. We assume they are identical in what follows. The flux ratio $R(\nu/\bar{\nu})$ is determined by extrapolating the ratio of $\bar{\nu}$ and ν quasielastic events to $Q^2 = 0$, where both cross sections are equal. The Pauli principle and finite resolution in determining Q^2 is taken into account by performing a Monte Carlo calculation of the integral $R(\nu/\bar{\nu})$ as a function of $Q_{\max}$ and using the experimental resolution in Q^2 and the Pauli principle with a degenerate Fermi gas with $P_f = 0.225$ GeV/c. The normalization of this curve is floated to fit the data. The fit yields the flux ratio $R(\nu/\bar{\nu}) = 0.47 \pm 0.05$.

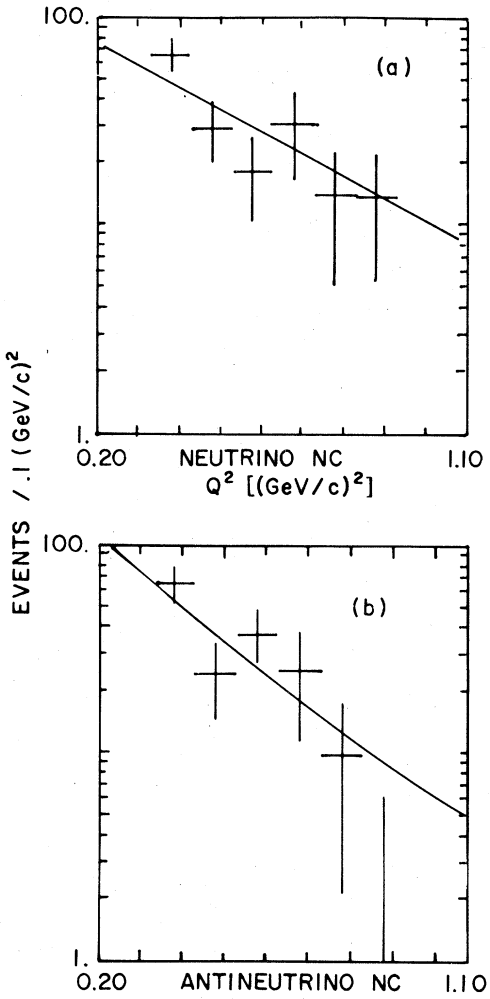

FIG. 3. Q^2 distributions for (a) $\nu_\mu p \rightarrow \nu_\mu p$ candidates and (b) $\bar{\nu}_\mu p \rightarrow \bar{\nu}_\mu p$ candidates satisfying 600 cuts. Residual neutron, wide-angle-muon, and single-pion events have been statistically subtracted. The solid line is the prediction of the Weinberg-Salam model with $M_A = 1.00$ GeV/c and $\sin^2\theta_W = 0.23$.

Results. The ratio

$$R_{\mathrm{NC}} = \sigma(\bar{\nu}p \to \bar{\nu}p)/\sigma(\nu p \to \nu p)$$

is given by

$$R_{\mathrm{NC}} = \frac{R(\nu/\bar{\nu})(N^{\bar{\nu}}_{\mathrm{obs}}/N^{\nu}_{\mathrm{obs}}) - f(\nu)}{1 - R(\nu/\bar{\nu})(N^{\bar{\nu}}_{\mathrm{obs}}/N^{\nu}_{\mathrm{obs}})f(\bar{\nu})} = 0.44 \pm 0.13 \ ,$$

where N^{ν}_{obs} and $N^{\bar{\nu}}_{\mathrm{obs}}$ are the final numbers in Table I and $f(\nu)$ and $f(\bar{\nu})$ are the fractional ν and $\bar{\nu}$ contaminations in the $\bar{\nu}$ and ν flux, respectively. The Q^2 distributions for ν and $\bar{\nu}$ events are shown in Fig. 3. We also form the ratio

$$R^{\mathrm{meas}}_{\nu_\mu} = \sigma(\nu p \to \nu p)/\sigma(\nu n \to \mu^- p) = 0.25 \pm 0.05 \ .$$

The NC and Q^2 distributions are in good agreement with the predictions of the Weinberg-Salam model for $\sin^2\theta_W = 0.2$–0.3 limits. $R^{\mathrm{meas}}_{\nu_\mu}$ is larger than expected. This effect can be understood, however, as the result of inclusion in the numerator of $\nu_\mu n \to \nu_\mu n$ events where the neutron charge exchanges in the aluminum nucleus. This effect is expected to cancel out in R_{NC} but is significant in $R^{\mathrm{meas}}_{\nu_\mu}$.

Because we are not able to separate $\nu_\mu n \to \nu_\mu n$ ($n \to p$) events from $\nu_\mu p \to \nu_\mu p$ events,

$$R^{\mathrm{meas}}_{\nu_\mu} = \frac{\sigma(\nu_\mu p \to \nu_\mu p) f_{p\to p} + \sigma(\nu_\mu n \to \nu_\mu n) f_{n\to p}}{\sigma(\nu_\mu n \to \mu^- p) f_{p\to p}} \ ,$$

where $f_{p\to p}$ is the probability that the proton emerges from the aluminum nucleus and is accepted into our sample, and $f_{n\to p}$ is the probability that a neutron charge exchanges in the nucleus and produces a proton accepted into our sample. $f_{n\to p}$ and $f_{p\to p}$ can be measured using our quasielastic ν and $\bar{\nu}$ data and out-of-time $np \to np$ events.[2] We find $f_{n\to p} = 0.28 \pm 0.05$ and $f_{p\to p} = 0.72 \pm 0.05$. Assuming

$$\sigma({}^{(-)}\nu_\mu n \to {}^{(-)}\nu_\mu n)/\sigma({}^{(-)}\nu_\mu p \to {}^{(-)}\nu_\mu p) = 1.5$$

(which is the case in the Weinberg-Salam model, independent of $\sin^2\theta_W$), we find $R^{\mathrm{corr}}_{\nu_\mu} = 0.11 \pm 0.03$.

In conclusion, we have measured ν_μ and $\bar{\nu}_\mu$ induced elastic scattering with significantly improved $\bar{\nu}_\mu$ statistics. The results are in agreement with the Weinberg-Salam model with $\sin^2\theta_W = 0.26 \pm 0.06$.

We would like to thank the staff of the Brookhaven National Laboratory AGS, and the University of Illinois and Nevis Laboratories scanning staffs for their outstanding work. This research was supported in part by the Department of Energy and the National Science Foundation. One of us (P.S.) acknowledges support of the Alfred P. Sloan Foundation.

---

[1]W. Lee *et al.*, Phys. Rev. Lett. 37, 186 (1976); D. Cline *et al.*, *ibid.* 37, 252 (1976); H. Faissner *et al.*, in *Neutrino '77*, proceedings of the International Conference on Neutrino Physics and Neutrino Astrophysics, Baksan Valley, U.S.S.R., 1977, edited by M. A. Markov, G. V. Domagatsky, A. A. Komar, and A. N. Tavkhelidze (Nauka, Moscow, 1978), p. 164; M. Pohl *et al.*, Phys. Lett. 72B, 489 (1978); A. Entenberg *et al.*, Phys. Rev. Lett. 42, 1198 (1979).

[2]Details of the determination of $f_{n\to p}$ and $f_{p\to p}$ can be found in P. Coteus, Ph.D. thesis, Nevis Report No. 236, 1981 (unpublished).